AAC Accepted Manuscript Posted Online 4 May 2020
Antimicrob. Agents Chemother. doi:10.1128/AAC.00530-20

Quercetin blocks Ebola Virus infection by counteracting the VP24 Interferon inhibitory function

Running title: Quercetin restores IFN cascade blocking EBOV infection

Elisa Fanunza[a*], Mathieu Iampietro[b], Simona Distinto[a], Angela Corona[a], Marina Quartu[c], Elias Maccioni[a], Branka Horvat[b], Enzo Tramontano[a,d]#

[a] *Department of Life and Environmental Sciences, University of Cagliari, Monserrato, Italy*

[b] *CIRI, International Center for Infectiology Research, CIRI, Univ Lyon, Inserm, U1111, University Claude Bernard Lyon 1, CNRS, UMR5308, Ecole Normale Supérieure de Lyon, Lyon, France*

[c] *Department of Biomedical Sciences, University of Cagliari, Monserrato, Italy*

[d] *Genetics and Biomedical Research Institute, National Research Council, Monserrato, Italy*

**Present address: Elisa Fanunza, Department of Biochemistry, Molecular Biology & Biophysics, University of Minnesota, Minneapolis, Minnesota, USA*

#Address correspondence to Enzo Tramontano, tramon@unica.it.

Word count for abstract: 224

Abstract

Ebola Virus (EBOV) is among the most devastating pathogens causing fatal hemorrhagic fever in humans. The 2013–2016 epidemics resulted in over 11000 deaths, while another outbreak is currently ongoing. Since there is no FDA-approved drug so far to fight EBOV infection, there is an urgent need to focus on drug discovery. Considering the tight correlation between the high EBOV virulence and its ability to suppress the type-I Interferon (IFN-I) system, identifying molecules targeting viral protein VP24, one of the main virulence determinants blocking IFN response, is a promising novel anti-EBOV therapy approach. Hence, in the effort of finding novel EBOV inhibitors, a screening of a small set of flavonoids was performed, showing that Quercetin and Wogonin can suppress the VP24 effect on IFN-I signaling inhibition. The mechanism of action of the most active compound, Quercetin, showing an IC_{50} value of 7.4 µM, was characterized to significantly restore the IFN-I signaling cascade, blocked by VP24, by directly interfering with the VP24 binding to karyopherin-α and thus restoring P-STAT1 nuclear transport and IFN genes transcription. Quercetin significantly blocked viral infection, specifically targeting EBOV VP24 anti-IFN-I function. Overall, Quercetin is the first identified inhibitor of the EBOV VP24 anti-IFN function, representing a molecule interacting with a viral binding site that is very promising for further drug development aiming to block EBOV infection at the early steps.

Keywords: Ebola virus; EBOV; VP24; IFN signaling; drug development, luciferase assay; flavonoids, quercetin.

Introduction

Within the *Filoviridae* family, the genus *Ebolavirus* consists of six species, Zaire, Sudan, Reston, Bundibugyo, Taï Forest and Bombali. The prototype Ebola virus (EBOV) belongs to the species *Zaire ebolavirus*, which is considered as the most virulent species resulting in up to 90% mortality. No FDA-approved drugs are available for Ebola Virus Disease (EVD) treatment. However, great efforts have been made in the development of EBOV therapeutics (1). In December 2019, the European Medicines Agency approved the first EBOV vaccine, Ervebo (2). Moreover, the Pamoja Tulinde Maisha (PALM) trial, in Congo, demonstrated the efficacy of two monoclonal antibody therapies, MAb114 and REGN-EB3, in reducing the case fatality rate of EVD (3).

The pathogenesis of EBOV disease involves the dysregulation of both the innate and adaptive immune system, allowing the virus to replicate, leading to the development of hematological manifestations, such as lymphopenia, thrombocytopenia, hemorrhage and finally death. In particular, the high virulence is tightly correlated to the suppression of the Interferon (IFN) response which represents the first line of defense during a viral infection (4, 5).

Together with EBOV VP35, the multifunctional protein VP24 is one of the main determinants of virulence by virtue of its inhibition of the IFN signaling cascade (4, 5). VP24 exerts its action by binding the NPI-1 subfamily of karyopherin-alphas (KPNα1, KPNα5 and KPNα6), importins involved in the nuclear transport of phosphorylated STAT1 (P-STAT1) protein, thus blocking the transcription of IFN stimulated genes (ISGs) (6–8). Recently, the crystal structure of the VP24/KPNα5 complex has been solved (PDB-ID: 4U2X) (9) showing that the KPNα5-VP24 binding region interface includes KPNα5 ARMs 7-10 and three VP24 clusters: Cluster 1 (N130, T131, N135, R137, T138 and R140), Cluster 2 (Q184, N185, H186) and Cluster 3 (L201, E203, P204, D205 and S207). Additional amino acids are required for the binding: L115, L121, D124, W125, T128 and T129 (9). Mutations of VP24 residues involved in the suppression of the IFN cascade were

shown to be responsible for the acquisition of high virulence in animal models (5, 10), suggesting VP24 as a validated target for drug development. Hence, identifying a therapy targeting the IFN-I inhibitory functions of EBOV represents a promising approach to an early control of the infection (11–14). A number of *in silico* studies reported molecules potentially able to bind different EBOV targets, including VP24 (15, 16), while two recent studies reported that a macrocyclic peptide and a nucleic acid aptamer could antagonize the binding of VP24 and KPNα in biochemical assays (17, 18). However, no small molecule has ever been reported to inhibit VP24 anti-IFN-I functions in cells and subsequent EBOV replication. Flavonoids have been described for their antiviral activity among the other biological properties (19), and a recent *in silico* study reported that few of them are able to form stable complexes with VP24 (16). Hence, using a recently developed drug screening assay (20), a small number of flavonoids were screened for their effect against VP24 observing that some of them were able to significantly inhibit VP24 anti-IFN-I activity, leading to the restoration of the IFN signaling cascade. In particular, Quercetin was shown to inhibit EBOV VP24 interaction with KPNα *in vitro* and to selectively inhibit EBOV infection.

Results

Gossypetin, Taxifolin and Tricetin Suppress VP24 IFN Inhibitory Function

A recent *in silico* docking study the flavonoids Gossypetin, Taxifolin and Tricetin (Figure 1A) were predicted to be potentially able to impair VP24 ability to disrupt the JAK/STAT signaling pathway (16). Hence, we wanted to verify whether these flavonoid derivatives were effectively able to affect VP24 anti-IFN-I function in a dual-luciferase reporter cell-based assay (20). In such assay, HEK293T cells were cotransfected with pISRE-luc, pRL-TK and a plasmid expressing EBOV VP24. The stimulation with IFN-α resulted in 100% of ISRE expression in mock-transfected cells, while cells cotransfected with VP24 showed an

inhibition of the IFN-I response. The treatment of VP24 cotransfected cells with 10 μM of Gossypetin, Taxifolin and Tricetin resulted in the partial restoration of the ISRE expression, demonstrating that all three compounds were able to block VP24 inhibitory effect on IFN signaling cascade in a cell-based assay, confirming *in silico* studies (Figure 1B).

Quercetin and Wogonin Are Active Compounds Against VP24

With the aim to identify more active compounds, we performed the screening of a small library of other eight flavonoids that share a similar structure with Gossypetin, Taxifolin and Tricetin. Utilization of a dual-luciferase reporter assay showed that two out of eight tested flavonoids, namely Quercetin and Wogonin (Figure 2A), significantly suppressed the anti-IFN function of VP24 restoring IFN stimulation (Figure 2B). In particular, at a concentration of 10 μM, Quercetin was able to restore ISRE expression from ~ 50% up to ~ 80%, in VP24 cotransfected cells, while Wogonin restored the pathway up to ~ 70% (Figure 2B). Overall, among all tested flavonoids Quercetin was the most effective in restoring the IFN stimulation (Figure 2B).

It has been demonstrated that some flavonoids, including the tested compounds Quercetin, Luteolin and Apigenin, are able to induce the interferon signaling (21, 22). Hence, in order to verify whether the tested flavonoids, at the indicated concentration, acted by targeting specifically VP24 or by enhancing the IFN response employing some VP24-independent mechanisms, we tested them for their ability to boost the IFN cascade protein (Figure 2C and 2D). Results demonstrated that none of the screened compounds enhanced the ISRE expression in HEK293T cells, confirming that active compounds could possibly specifically interact with VP24. Of note, Myricetin and Dihydromyricetin reduced ISRE activation (Figure 2D). In fact, Myricetin has been reported to inhibit STAT1 phosphorylation (23), and this can explain the inhibition of the ISRE transcription. While no

direct data are available for Dihydromyricetin, and considering its structural diversity from Myricetin, further studies are needed to understand its mechanism of action.

Quercetin dose-dependently blocks VP24 Inhibition of ISRE Expression and Affects ISG15 mRNA Transcription

Next, we wanted to better evaluate the effect of the most active compound, Quercetin, on the VP24 blockade of the IFN signaling by performing a dose-response curve in the presence of the same amount of VP24 plasmid. Of note, Quercetin exhibited a dose-dependent reversion of the VP24 inhibition of the ISRE IFN-dependent stimulation showing an IC_{50} value of 7.4 μM (Figure 3A). Quercetin cytotoxicity in HEK293T cells was also assessed, yielding 100% cell viability at concentrations between 3 μM and 30 μM and a CC_{50} value >100 μM (Figure 3B), hence Quercetin showed a selectivity index (SI, CC_{50}/IC_{50}) >13. We then wanted to examine the effect of Quercetin on the modulation of IFN signaling by VP24 using a different end-point, i.e. by assessing its efficacy on the ISG15 gene expression. The analysis confirmed that VP24 was effectively able to inhibit ISG15 mRNA transcription in IFN-stimulated cells as compared to cells transfected with an empty vector (Figure 3C). These results also confirmed that Quercetin significantly restored the IFN-induced ISG15 gene expression down-regulated by VP24, confirming that the compound was effectively blocking VP24 function (Figure 3C).

Quercetin Blocks VP24 Inhibition of P-STAT1 Nuclear Transport

It is well known that VP24 inhibits the translocation of P-STAT1 to the nucleus (6–8). With the aim of verifying whether Quercetin could increase the P-STAT1 nuclear transport, we performed an immunofluorescence assay by stimulating cells with a high amount of IFN-α (150 ng/mL) for 30 minutes, with or without Quercetin. As expected, in control cells

transfected with an empty vector, 100% of IFN-stimulated cells were positive for nuclear P-STAT1, indicating the activation of the IFN signaling cascade after IFN-α stimulation (Figure 4A and 4B). Differently, in IFN-stimulated cells expressing VP24 after transfection, P-STAT1 nuclear transport was inhibited, as no P-STAT1 was detectable in the nuclei of these cells (Figure 4A). In this system, the presence of Quercetin in IFN-stimulated VP24 transfected cells led to a significant increase (20%) of cells positive for nuclear P-STAT1 (Figure 4A and 4B). Of note, this also showed that Quercetin was able to rapidly block the VP24 anti-IFN function.

In silico and _In vitro_ Characterization of Quercetin Binding Mode on VP24-KPNα Complex

We performed *in silico* molecular docking experiments to evaluate the putative binding mode of Quercetin on VP24. Among the available VP24 crystal structures, 4M0Q (24) currently has the best resolution (1.92 Å) and, therefore, it was selected for docking experiments performed by means of Glide-XP (25). Then, the best docking complexes were subjected to a post-docking procedure based on energy minimization applying molecular mechanics generalized Born/surface area (MM-GBSA) method and continuum solvation models (26). The most stable binding mode was analyzed showing that Quercetin occupies a central position in the reported contact area between VP24 and KPNα5 (Figure 5A). The complex VP24-Quercetin resulted to be stabilized by hydrogen bonds with the VP24 key residues N130, L201, E203, while additional residues are involved in anchoring the compound i.e L127, W92 by hydrogen bonds and K218 by cation-π interaction (Figure 5B). Such *in silico* analysis allowed to propose that the presence of Quercetin in such a VP24 pocket, would prevent KPNα5 ARMs 7-10 to move close to VP24, ultimately inhibiting the VP24 binding to KPNα5 (Figure 5C).

To demonstrate that Quercetin was effectively able to interfere with the binding between VP24 and KPNα, co-immunoprecipitation assays were performed. Cells were cotransfected with a V5-tagged VP24 and a FLAG-tagged KPNα1 and, one day post-transfection, after stimulation with IFNα and treatment with Quercetin, lysates were precipitated with anti-FLAG magnetic beads and immunocomplexes analyzed by Western blotting (Figure 5D and 5E). As expected, FLAG-KPNα1 was coprecipitated with V5-VP24. When VP24 cotransfected cells were treated with Quercetin, there was a significant reduction in VP24 co-immunoprecipitated with KPNα1 (Figure 5E). This result indicates that Quercetin is indeed able to interfere with the binding between VP24 and KPNα1, confirming the proposed *in silico* model.

Antiviral Activity of Quercetin Against EBOV Replication

It has been recently demonstrated that Quercetin 3-β-O-D-glucoside (Q3G), a glucosylated form of quercetin, has antiviral activity against EBOV both *in vitro* and *in vivo* (27). In order to test if also Quercetin was able to inhibit EBOV replication, wild-type EBOV-Makona infected cells were treated with Quercetin, Q3G and IFNα as a control for inhibition. We showed that Quercetin significantly inhibited the viral replication in HEK293T cells (Figure 6A), while it was not able to inhibit EBOV in VeroE6 cells (Figure 6C). EBOV yield in supernatants collected from HEK293T cells treated with the compounds was also significantly reduced (Figure 6B), while the antiviral effect of Quercetin in supernatant from Vero cells was not significant (Figure 6D). Indeed, as expected, the lack of effect of Quercetin on EBOV replication in Vero cells confirmed the proposed mode of action since Vero E6 cannot produce type I IFNs and thus the JAK-STAT cascade, in total absence of exogenous IFN, is not activated and, hence, VP24 cannot exert its interferon inhibitory function (28). In contrast to Quercetin, Q3G was able to block EBOV replication in both cell lines (Figure 6). It has been previously demonstrated that Q3G targets the viral entry

206 process (27). The fact that Q3G is more active in HEK293T as compared to Vero cells
207 might suggest a dual mechanism of action: 1) impairing the IFN antagonism of VP24, and
208 2) a mechanism independent of that, as proposed by Qiu et al. (27), blocking the level of
209 virus entry.

210 To exclude that the decrease in viral titers was attributed to cells toxicity, we measured
211 Quercetin and Q3G cytotoxicity, observing that in both HEK293T and VeroE6 cells their
212 CC_{50} value was > 100 uM (data not shown). Furthermore, we performed a Western
213 blotting examining the level of caspase 3 cleavage as marker of apoptosis (29). We used
214 antibodies recognizing the caspase 3 active cleaved form and its inactive precursor, and
215 we observed that no relevant cleaved caspase 3 was detectable in any of the tested
216 samples, despite the expression of high amounts of its inactive precursor protein (Figures
217 6E and 6F). Given the absence of apoptosis, we confirmed that the reduction in viral
218 replication was only due to compounds treatment.

219 Finally, to confirm this hypothesis, we investigated if Q3G, like the not glucosylated form,
220 was able to revert the ISRE expression in HEK293T. VP24 transfected cells were
221 stimulated with IFN-α and treated with increasing concentration of Q3G. We observed that
222 also Q3G dose-dependently inhibited VP24 IFN inhibitory function with an IC_{50} of 9.5 μM
223 (Figure 7A) showing no alternative VP24-independent mechanism on ISRE stimulation
224 (Figure 7B) and no cytotoxicity even at high concentrations (Figure 7C). Similarly to
225 Quercetin, Q3G was able to restore the P-STAT1 nuclear transport in VP24 cotransfected
226 cells resulting in a significant 17% of nuclear P-STAT1 positive cells (Figure 7D). Given the
227 similar IC_{50} for Quercetin and Q3G, we hypothesized that the presence of the glucoside
228 was not altering the binding of the molecule with VP24. Indeed, performing the alignment
229 of Quercetin-VP24 and Q3G-VP24 complexes, obtained by docking analysis with VP24,
230 we confirmed that the glucoside moiety was not altering the position of the Q3G, as
231 compared to Quercetin, on VP24 (Figure 7E and 7F). In addition, co-IP of VP24 and

KPNα1 in cells treated with Q3G, showed that the compound was affecting the binding between VP24 and the importin, resulting in a 20% reduction of co-immunoprecipitated VP24, as compared to the untreated control (Figure 7G). These results suggest that Q3G is slightly less efficient as compared to the not glucosylated form.

Discussion

Among the diversified antiviral strategies developed to counteract the different steps of the viral life cycle (30–34), interfering with the initial phases of infection, such as the viral evasion of the IFN system, is an attractive therapeutic approach against several types of viruses (35–38). Since the EBOV inhibition of IFN response massively contributes to the viral pathogenesis (4, 5), restoring the IFN system could represent a promising strategy for EBOV control (13). Two viral proteins have been demonstrated to suppress interferon responses, VP35 and VP24 (13, 39). Different studies have shown that it is possible to block the VP35 IFN inhibitory function with natural compounds (11, 12) and also antibodies (14), thus restoring the IFN production cascade. Recently, Jasenosky *et al*. demonstrated that the known FDA approved small molecule Nitazoxanide was able to significantly suppress EBOV replication in human cells through enhancing the RIG-I pathway sensing, thus counteracting EBOV VP35's ability to prevent the triggering of the host antiviral response (40).

Although several mutational studies confirmed VP24 as a validated therapeutic target (15, 16, 41–44), up to now, only two molecules have been reported to block the binding between VP24 and KPNα that is essential for the anti-IFN VP24 function (17, 18). Firstly, using the RaPID system, that allows the selection of high-affinity binders from an mRNA library of non-standard peptides, Song *et al*. were able to identify a macrocyclic peptide binder for VP24, namely eVpeD2.This represents the first molecule that has been

258 shown to inhibit the VP24–KPNα5 protein–protein interaction with an IC_{50} value of 9 μM
259 (17). Secondly, natural and artificial nucleic acid aptamers with high-affinity for VP24 were
260 generated using the capillary electrophoresis-systematic evolution of ligands by
261 exponential enrichment (CE-SELEX). Sharing a common binding site with KPNα1, they
262 compete for the binding with VP24 (Kd ≈ 0.1 nM) (18). Even though they show to be active
263 at micromolar and sub-nanomolar range in biochemical assays, at the best of our
264 knowledge, they have not been reported to be tested in cell-based assays.

265 The identification of compounds able to block VP24 functions in human cells was
266 previously limited due to the difficulty of developing a suitable cellular screening system.
267 We firstly developed a cellular model able to evaluate the inhibition of IFN signaling by
268 VP24 (20) and, secondly, we used this system to test anti-VP24 agents. Differently from
269 biochemical assays, cell-based assays can be used to monitor specific viral proteins and
270 pathways, such as VP24 and the ISRE expression, providing the means to test for potent
271 viral inhibitors intracellularly, thus giving extra information about their effect inside the more
272 complex cellular context, improving the early phase of the drug-discovery process.

273 Since previous *in silico* studies suggested the potential anti-EBOV activity of
274 flavonoid derivatives, we performed a screening of different flavonoids in cell-based assay.
275 It has been shown that flavonoids possess a wide range of biological properties such as
276 antioxidant, hepatoprotective, antibacterial, anti-inflammatory (19, 45), and antiviral
277 activities against different viruses such as Japanese encephalitis virus (46), Dengue virus
278 type-2 (47), Influenza virus (48, 49), Human immunodeficiency virus (50, 51). Different
279 modes of action have been proposed such as the inhibition of viral polymerase and capsid
280 proteins by flavonoids (52).

281 In the present study, we aimed to characterize the flavonoids effect on the IFN
282 inhibition mediated by VP24 and observed that Quercetin and Wogonin were able to inhibit
283 VP24 significantly, restoring the ISRE expression, with Quercetin being the most active

284 compound. Quercetin is a molecule largely present in the human diet being part of many
285 fruits and vegetables. It has been reported that up to 1 g average intake of quercetin
286 occurs a day, and thus represents 60 to 75% of the overall polyphenols' ingestion (53).
287 Among its wide range of biological activities, it has been demonstrated to be active on
288 different viruses, including HCV (54), Mayaro virus (55), IAV (56), CHIKV (57) and EBV
289 (58). In particular, Quercetin has been shown to inhibit HCV through the binding and
290 inactivating the viral NS3 protease (59), Zandi et al. proposed that Quercetin prevents
291 DENV-2 replication by inhibiting viral RNA polymerase (47) and a recent paper by Granato
292 et al. suggested that Quercetin may have potential to be used to counteract EBV-driven
293 lymphomagenesis, since it is able to counteract EBV-driven immortalization of B cells and
294 LCL outgrowth, interrupting the crosstalk between IL-6 and STAT3 and promoting
295 autophagy (60). Moreover, a Quercetin derivative, Q3G, has been demonstrated to inhibit
296 the early steps of EBOV entry (27). Our results provide a novel antiviral mechanism
297 adopted by Quercetin and its derivative Q3G. In fact, we observed that Quercetin inhibits
298 EBOV VP24 leading to a partial restoration of the ISRE expression, ISG15 mRNA
299 transcription and the P-STAT1 nuclear transport in presence of the viral protein. Docking
300 studies suggest the putative Quercetin binding mode at the interface between VP24 and
301 KPNα5. The binding of a small molecule in this surface could prevent KPNα binding. This
302 mechanism was confirmed by the ability of Quercetin to affect the binding of co-
303 immunoprecipitated KPNα and VP24.

304 We also tested the effect of Quercetin on EBOV replication, demonstrating that the
305 compound was able to significantly suppress viral replication. This effect was similar to
306 previously reported effect of flavonoid derivative Q3G (27). Contrarily to Q3G, however,
307 the effect of Quercetin was not due to an inhibition of the entry process, since Quercetin
308 only inhibited EBOV in IFN-competent HEK293T, being not effective in IFN-incompetent
309 Vero cells. This result supports the hypothesis that Quercetin is affecting specifically the

EBOV evasion of the IFN pathway. Differently, Q3G inhibited EBOV replication in both cell lines, and its more potent effect on HEK293T, as compared to the one measured on Vero E6 cells, possibly suggests a bimodal mechanism. In fact, when Q3G was tested in our cell-based assay, we observed that the glucosylated molecule was able to inhibit EBOV VP24 by reverting both the IFNα-induced stimulation and the P-STAT1 nuclear translocation blocked by the viral protein. Molecular docking experiments confirmed that Q3G was localizing in the same VP24 surface as Quercetin, suggesting that also Q3G is affecting the binding between VP24 and KPNα, however with lower efficiency. In addition, present data suggest that the glucoside moiety is probably required for the inhibition of viral entry, since this mechanism was not observed for the aglycone form.

In conclusion, we identified a small molecule, already used as a nutritional supplement, for which toxicity and pharmacokinetics are well known (53), whose metabolism is well studied in animal models and that is a promising anti-EBOV agent. In fact, it has been previously demonstrated that after only 2 hours of Quercetin orally administration (50 and 100 mg/kg body weight) the total Quercetin plasma concentrations in mice, rats and gerbils reached concentrations between 6–12 μM (61). The molecule could rapidly exert its anti-EBOV activity either in plasma (mainly for the indirect effect of its metabolite, Q3G, as previously reported by *Qiu et al.*) (27) and also in tissues where Q3G is again converted into its aglycone form.

Quercetin is the first compound that specifically inhibits EBOV VP24 IFN-inhibitory function, restoring the IFN signaling cascade and leading to the block of viral infection. Given its good tolerability, these findings open original perspectives in the field of the EBOV therapeutics development.

Materials and Methods

335 **Cells and Reagents.** HEK293T cells were cultured in Dulbecco's modified Eagle's
336 medium (Gibco) supplemented with 10% fetal bovine serum (Gibco) and 1%
337 penicillin/streptomycin (Sigma). pISRE-luc and pcDNA3.1-FLAG-VP24 were kindly gifted
338 by Prof Ian Goodfellow (University of Cambridge, UK) and Marco Sgarbanti (Italian
339 National Institute of Health, Italy), respectively. pcDNA3-V5-VP24 and FLAG-tagged
340 KPNα1 were provided by Dr St Patrick Reid (University of Nebraska Medical Center,
341 USA). pRL-TK plasmid, T-Pro P-Fect Transfection Reagent and Human Recombinant IFN-
342 α were purchased from Promega, T-Pro Biotechnology and PeproTech, respectively.
343 Gossypetin, Taxifolin, Tricetin were from Extrasynthese, while Q3G, Myricetin,
344 Dihydromyricetin, Luteolin, Apigenin, Quercitrin, Quercetin, Wogonin, Baicalein, Anti-FLAG
345 M2 antibodies and anti-FLAG magnetic beads were from Sigma-Aldrich. Antibodies
346 against P-STAT1, glyceraldehyde-3-phosphate dehydrogenase (GAPDH), anti-caspase-3,
347 anti-cleaved caspase-3 and the HRP-linked IgG were purchased from Cell Signaling.
348 Alexa Fluor 488 goat anti-mouse IgG, Alexa Fluor 594 goat anti-rabbit IgG and Pierce ECL
349 Western Blotting Substrate were from Thermo Fisher Scientific.
350
351 **Virus.** Zaïre EBOV (Makona strain) (62) was prepared by infecting Vero E6 cells and
352 titrated on Vero E6 cells as well by plaque assay, using crystal violet in the INSERM Jean
353 Mérieux BSL-4 laboratory in Lyon, France. 293T and VeroE6 cells were cultured in
354 Dulbecco's modified Eagle's medium (DMEM) GlutaMAX (LifeTechnologies)
355 supplemented with 10% heat inactivated fetal bovine serum (HI-FBS) (Eurobio), 1%
356 HEPES, 1% nonessential amino acids, 1% sodium pyruvate, and 2% penicillin-
357 streptomycin mix (all LifeTechnologies). For treatments and infections, cells were plated in
358 12-well plates at $2.5.10^5$ cells per well, then cells were treated with DMSO (Sigma Aldrich),
359 Quercetin (30 µM) (Sigma Aldrich), Q3G (10 µM) (Sigma Aldrich) or IFNα (1000 IU/ml)
360 (PBL Assay Science) for 1h at 37°C before being infected or not with EBOV Makona at a

MOI of 0.1 PFU/cell for 1h at 37°C. Then, virus-containing media were removed, and cells were washed with PBS1X. Furthermore, fresh DMEM media containing drugs associated to each condition as described previously was added to cells that were incubated for 72h at 37°C. Finally, infected cell lysates and supernatants were collected for further analysis, according to validated BSL-4 procedures.

VP24 IFN Inhibition Assay. EBOV VP24 inhibition of the ISRE dependent promoter reporter plasmid (pISRE-luc) after IFN-α stimulation has been previously described (20). Briefly, HEK293T cells were cotransfected, using T-pro P-Fect transfection reagent with pISRE-luc (60 ng/well), a constitutively expressed Renilla luciferase reporter plasmid (RL-TK) (10 ng/well) and a FLAG-tagged wild-type VP24 plasmid (30 ng/well) from the Zaire Ebolavirus isolate H.sapiens-wt/GIN/2014/Gueckedou-C05, Sierra Leone/guinea strain. Renilla luciferase was used to normalize transfection efficiencies. Twenty-four hours post-transfection, cells were mock or IFN-α stimulated (1 ng/mL) and treated or not with compounds (3 µM, 10 µM, 30 µM, 100 µM) for 8 hours. Then luciferase reporter activities were analyzed using cell lysates and luciferase counts were determined using a Victor3 luminometer.

IC_{50} Calculation. To determine the IC_{50} of Quercetin, we used the log agonist concentration versus response, variable slope algorithm in GraphPad Prism software where $Y = Bottom + (Top-Bottom)/(1+10\hat{}((LogIC_{50})))$. IC_{50} values were calculated based on three independent experiments performed in triplicate.

Cell viability assays. HEK293T and Vero E6 cells were seeded in 96-well plates. After 24 h, cells were treated with Quercetin and Q3G and incubated 8 h or 72 h at 37 °C in 5% CO_2. Then, Presto Blue Cell Viability Reagent (Thermo Fisher Scientific) was added to

each well. The plate was incubated for 1 h at 37 °C in 5% CO2 and fluorescence was read in the Victor3 luminometer.

After 72h of infection, HEK293 T and Vero E6 cells treated and not treated were harvested, washed three times with PBS and lysed in RIPA lysis buffer (ThermoScientific) supplemented with 4X LAEMMLI buffer (LifeTechnologies) and 10X reducing agent buffer (Invitrogen). Then, Western blot analysis was performed using anti-caspase-3 (Cell Signaling) and anti-cleaved caspase-3 (Cell Signaling) antibodies. GAPDH antibody (EMD Millipore) was used as internal control gene.

Immunofluorescence. For immunostaining, HEK293T cells, grown in 6 well plates on glass slides, were cotransfected with Lipofectamine 2000 transfection reagent (Invitrogen) with pcDNA3.1 (2.5 µg/well) or EBOV VP24 plasmid (2.5 µg/well). After 24 h of transfection, cells were treated with IFN-α (150 µg/well) for 30 minutes and then fixed with 4% paraformaldehyde in PBS for 15 minutes at RT. Permeabilization was performed with ice-cold 100% methanol for 10 minutes, washed with PBS, and blocked in blocking buffer (PBS containing 0.2% Triton X-100, 10% normal goat serum and 3% bovine serum albumin) for 1 h at room temperature (RT). Cells were firstly incubated with mouse anti-Flag (Sigma-Aldrich)(1:500) and rabbit anti-P-STAT1 (Cell signaling)(1:400) for 1 h at RT, and then with goat anti-mouse and anti-rabbit secondary antisera conjugated with Alexa Fluor 488 and Alexa Fluor 594 (Invitrogen) (1:500), for 1 h at RT. After incubation with the nuclear dye Hoechst 33258 (Sigma-Aldrich), slides with stained cells were mounted on histology standard slides with Glycerol Mounting Medium with 1,4-diazabicyclo[2.2.2]octane (DABCO) as anti-fading reagent, observed with an Olympus BX61 microscope, equipped with epifluorescence illumination, and digital images were captured with a Leica DF 450C camera. The cultures were examined at 40x magnification. Cells were counted using the Cell Counter plugin image analysis program ImageJ.

RNA Extraction and Quantitative Real-Time PCR. Total RNA was extracted from transfected cells with TRIzol reagent (Invitrogen). RNA was then reverse transcribed and amplified using Luna Universal One-Step RT-qPCR kit (New England Biolabs). Quantitative real-time PCR (RT-qPCR) experiments were performed in triplicate. mRNA expression levels were normalized to the level of GAPDH. Results are expressed as percentage of mRNA transcript levels of treated cells versus not treated cells. Regarding BSL-4 procedures, total RNAs from cells and supernatants were inactivated with RLT and AVL reagents (Qiagen) respectively before being extracted using the Nucleospin RNA kit (Macherey-Nagel). Reverse transcription was realized using iScript cDNA kit (Bio-Rad) and qPCR were realized using Platinium SYBR Green qPCR SuperMix-UDG kit with ROX (Invitrogen). Data were treated using StepOne software and calculations were done using the $2^{\Delta\Delta CT}$ method and normalized with GAPDH house-keeping gene. Primers used for qPCR are EBOV Makona NP forward (GCT CCT TTC GCC CGA CTT TTG AA) and EBOV Makona NP reverse (CTG TGG CGA CTC CGA GTG CAA).

Co-immunoprecipitation experiment. HEK293T cells were transfected with empty or expression plasmids for V5 tagged VP24 and FLAG-tagged KPNα1 and lysed in PBS containing 1.5% Triton X-100, 1 mM Na_3VO_4, 1mM DTT and 1x cOmplete protease inhibitor cocktail (Roche). Lysates were incubated with anti-FLAG M2 magnetic beads overnight at 4°C. Precipitated proteins were eluted by boiling with SDS sample loading buffer. Whole cell lysates and immunoprecipitated samples were analyzed by Western blotting. Membranes were probed with anti-FLAG M2 (Sigma-Aldrich, 1μg/mL), anti-V5 (Thermo Fisher Scientific, 1:200) and anti-GAPDH (Cell Signaling, 1:1000). Images were captured with Chemidoc MP Imaging System (Bio-Rad). Bands quantification was performed using Image Lab software. Co-immunoprecipitated V5-VP24 was normalized to

439 the level of immunoprecipitated FLAG-KPNα1. V5-VP24 and KPNA bands in WCL were
440 normalized to the level of GAPDH.
441
442 **Molecular Docking. Ligand Preparation.** The 2D coordinate structure-data file (SDF) file
443 of Quercetin and Q3G ligands were downloaded from Pubchem compound repository.
444 Then, they were prepared with Maestro GUI and subject to conformational analysis by
445 means of MacroModel program version 9.2 (63). Merck molecular force fields (MMFFs)
446 (64) was applied as force field and it was considered the implicit solvation model
447 Generalized Born/Surface Area (GB/SA) water (26). Therefore the compounds geometry
448 was energy minimized using Polak-Ribier Conjugate Gradient (PRCG) method, 5000
449 iterations and a convergence criterion of 0.05 kcal/(mol Å). The compounds global
450 minimum conformations were considered for the docking studies. **Docking Protein**
451 **Preparation.** The coordinates for VP24 were taken from the RCSB Protein Data Bank (65)
452 considering the pdb model 4M0Q (24). The protein was prepared by means of Maestro
453 Protein Preparation Wizard (Maestro, Schrödinger L. L. C., New York, N., USA, 2018).
454 Original water molecules were removed. The bond orders, hydrogen atoms and formal
455 charges were added in the structure. After preparation, the structure was refined in order
456 to optimize the hydrogen bond network using OPLS_2005 force field (66). **Docking**
457 **Experiments.** Docking inner and outer grids were defined around the refined structure by
458 calculating the centroid of clustered residues interacting with KPNα5 (9). The coordinates
459 Grid point's level for x, y, z axis are -2,06, -21,53, -12,16. The inner box side was
460 increased to 15 Å while the outer was left of 20 Å. The box resulted a cube of 35 Å for side
461 in order to include the whole protein. The extra precision (XP) docking algorithm was
462 applied for scoring theoretical poses (25). The other settings were left as default. **Post-**
463 **Docking.** In order to better take into account, the induced fit phenomenon occurring at the
464 ligand binding domain, the most energy favored generated complexes were fully optimized

with 10000 steps of the Polak-Ribier conjugate gradient (PRCG) minimization method considering OPLS_2005 force field and GB/SA implicit water. The optimization process was performed up to the derivative convergence criterion equal to 0.1 kJ/(mol*Å).

Statistical analysis and graphic visualization. Statistics and graphics were performed using GraphPad Prism software 6.01 (GraphPad software, Inc, 2012), Pymol (The PyMOL Molecular Graphics System Version1.7, Schrödinger, L. L. C.) and Maestro Ligand Interaction visualization (Maestro, Schrödinger L. L. C., New York, N., USA, 2018).

Acknowledgments

The present study was supported by RAS LR 07/2007 grant n. CRP-78711/F72I15000900002.

EF and ET conceived, designed the experiments and wrote the paper; EF, MI, SD performed the experiments; EF, MI, AC, MQ, EM and BH analyzed data. All authors revised the manuscript and read and approved the final version. We thank Claire Dumont for her technical support.

The authors declare no conflict of interest.

References

1. Fanunza E, Frau A, Corona A, Tramontano E. 2018. Antiviral Agents Against Ebola Virus Infection: Repositioning Old Drugs and Finding Novel Small MoleculesAnnual Reports in Medicinal Chemistry.
2. Henao-Restrepo AM, Longini IM, Egger M, Dean NE, Edmunds WJ, Camacho A, Carroll MW, Doumbia M, Draguez B, Duraffour S, Enwere G, Grais R, Gunther S, Hossmann S, Kondé MK, Kone S, Kuisma E, Levine MM, Mandal S, Norheim G,

Riveros X, Soumah A, Trelle S, Vicari AS, Watson CH, Kéïta S, Kieny MP, Røttingen JA. 2015. Efficacy and effectiveness of an rVSV-vectored vaccine expressing Ebola surface glycoprotein: interim results from the Guinea ring vaccination cluster-randomised trial. Lancet 386:857–66.

3. Mulangu S, Dodd LE, Davey RT, Mbaya OT, Proschan M, Mukadi D, Manzo ML, Nzolo D, Oloma AT, Ibanda A, Ali R, Coulibaly S, Levine AC, Grais R, Diaz J, Clifford Lane H, Muyembe-Tamfum JJ, Sivahera B, Camara M, Kojan R, Walker R, Dighero-Kemp B, Cao H, Mukumbayi P, Mbala-Kingebeni P, Ahuka S, Albert S, Bonnett T, Crozier I, Duvenhage M, Proffitt C, Teitelbaum M, Moench T, Aboulhab J, Barrett K, Cahill K, Cone K, Eckes R, Hensley L, Herpin B, Higgs E, Ledgerwood J, Pierson J, Smolskis M, Sow Y, Tierney J, Sivapalasingam S, Holman W, Gettinger N, Vallée D, Nordwall J. 2019. A randomized, controlled trial of Ebola virus disease therapeutics. N Engl J Med 382:2293–2303.

4. Prins KC, Delpeut S, Leung DW, Reynard O, Volchkova VA, Reid SP, Ramanan P, Cárdenas WB, Amarasinghe GK, Volchkov VE, Basler CF. 2010. Mutations Abrogating VP35 Interaction with Double-Stranded RNA Render Ebola Virus Avirulent in Guinea Pigs. J Virol 84:3004–3015.

5. Ebihara H, Takada A, Kobasa D, Jones S, Neumann G, Theriault S. 2006. Molecular Determinants of Ebola Virus Virulence in Mice. PLoS Pathog 2:1–7.

6. Reid SP., Leung LW., Hartman AL., Martinez O., Shaw ML., Carbonnelle C., Volchkov VE., Nichol ST., Basler CF. D. 2006. Ebola virus VP24 binds karyopherin α1 and blocks STAT1 nuclear accumulation. J Virol 80:5156–5167.

7. Mateo M, Reid SP, Leung LW, Basler CF, Volchkov VE. 2010. Ebolavirus VP24 binding to karyopherins is required for inhibition of interferon signaling. J Virol 84:1169–75.

8. Reid SP, Valmas C, Martinez O, Mauricio Sanchez F, Basler CF. 2007. Ebola Virus

VP24 Proteins Inhibit the Interaction of NPI-1 Subfamily Karyopherin α Proteins with Activated STAT1. J Virol 81:13469–13477.

9. Xu W, Edwards MR, Borek DM, Feagins AR, Mittal A, Pappu R V, Leung DW, Basler CF, Amarasinghe GK. 2015. Ebola virus VP24 targets a unique NLS binding site on karyopherin alpha 5 to selectively compete with nuclear import of phosphorylated STAT1. 16:187–200.

10. Volchkov VE, Chepurnov AA, Volchkova VA, Ternovoj VA, Klenk H. 2000. Molecular Characterization of Guinea Pig-Adapted Variants of Ebola Virus. Virology 277:147–155.

11. Di Petrillo A, Fais A, Pintus F, Santos-Buelga C, González-Paramás AM, Piras V, Orrù G, Mameli A, Tramontano E, Frau A. 2017. Broad-range potential of Asphodelus microcarpus leaves extract for drug development. BMC Microbiol 17:159.

12. Daino GL, Frau A, Sanna C, Rigano D, Distinto S, Madau V, Esposito F, Fanunza E, Bianco G, Taglialatela-Scafati O, Zinzula L, Maccioni E, Corona A, Tramontano E. 2018. Identification of Myricetin as an Ebola Virus VP35-Double-Stranded RNA Interaction Inhibitor through a Novel Fluorescence-Based Assay. Biochemistry 57:6367–6378.

13. Fanunza E, Frau A, Corona A, Tramontano E. 2018. Insights into Ebola Virus VP35 and VP24 Interferon inhibitory functions and their initial exploitation as drug targets. Infect Disord - Drug Targets 19:362–374.

14. Flego M, Frau A, Accardi L, Mallano A, Ascione A, Gellini M, Fanunza E, Vella S, Di Bonito P, Tramontano E. 2019. Intracellular human antibody fragments recognizing the VP35 protein of Zaire Ebola filovirus inhibit the protein activity. BMC Biotechnol 19:64.

15. Plesko S, Volk H, Luksic M, Podlipnik C. 2015. In Silico Study of Plant Polyphenols ’

Interactions with VP24 – Ebola Virus Matrix Protein In Silico Study of Plant Polyphenols ' Interactions with VP24 – Ebola Virus Membrane-associated Protein. Acta Chim Slov 62:555–64.

16. Raj U, Varadwaj PK. 2016. Flavonoids as Multi-target Inhibitors for Proteins Associated with Ebola Virus: In Silico Discovery Using Virtual Screening and Molecular Docking Studies. Interdiscip Sci Comput Life Sci 8:132–141.

17. Song X, Lu L, Passioura T, Suga H. 2017. Macrocyclic peptide inhibitors for the protein–protein interaction of Zaire Ebola virus protein 24 and karyopherin alpha 5. Org Biomol Chem 15:5155–5160.

18. Tanaka K, Kasahara Y, Miyamoto Y, Takumi O, Kasai T, Onodera K, Kuwahara M, Oka M, Yoneda Y, Obika S. 2018. Development of oligonucleotide-based antagonists of Ebola virus protein 24 inhibiting its interaction with karyopherin alpha 1. Org Biomol Chem 16:4456–4463.

19. Kumar S, Pandey AK. 2013. Chemistry and biological activities of flavonoids: An overview. Sci World J.

20. Fanunza E, Frau A, Sgarbanti M, Orsatti R, Corona A, Tramontano E. 2018. Development and Validation of a Novel Dual Luciferase Reporter Gene Assay to Quantify Ebola Virus VP24 Inhibition of IFN Signaling. Viruses 10:98.

21. Tai Z, Lin Y, He Y, Huang J, Guo J, Yang L, Zhang G, Wang F. 2014. Luteolin sensitizes the antiproliferative effect of interferon α/β by activation of janus kinase/signal transducer and activator of transcription pathway signaling through protein kinase A-mediated inhibition of protein tyrosine phosphatase SHP-2 in cance. Cell Signal 26:619–628.

22. Igbe I, Shen X-F, Jiao W, Qiang Z, Deng T, Li S, Liu W-L, Liu H-W, Zhang G-L, Wang F. 2017. Dietary quercetin potentiates the antiproliferative effect of interferon-α in hepatocellular carcinoma cells through activation of JAK/STAT pathway

signaling by inhibition of SHP2 phosphatase. Oncotarget 8:113734–113748.

23. Scarabelli TM, Mariotto S, Abdel-Azeim S, Shoji K, Darra E, Stephanou A, Chen-Scarabelli C, Marechal JD, Knight R, Ciampa A, Saravolatz L, de Prati AC, Yuan Z, Cavalieri E, Menegazzi M, Latchman D, Pizza C, Perahia D, Suzuki H. 2009. Targeting STAT1 by myricetin and delphinidin provides efficient protection of the heart from ischemia/reperfusion-induced injury. FEBS Lett 583:531–541.

24. Edwards MR, Johnson B, Mire CE, Xu W, Shabman RS, Speller LN, Leung DW, Geisbert TW, Amarasinghe GK, Basler CF. 2014. The Marburg Virus VP24 Protein Interacts with Keap1 to Activate the Cytoprotective Antioxidant Response Pathway. Cell Rep 6:1017–1025.

25. Friesner RA, Murphy RB, Repasky MP, Frye LL, Greenwood JR, Halgren TA, Sanschagrin PC, Mainz DT. 2006. Extra precision glide: Docking and scoring incorporating a model of hydrophobic enclosure for protein-ligand complexes. J Med Chem 49:6177–6196.

26. Kollman PA, Massova I, Reyes C, Kuhn B, Huo S, Chong L, Lee M, Lee T, Duan Y, Wang W, Donini O, Cieplak P, Srinivasan J, Case DA, Cheatham TE. 2000. Calculating structures and free energies of complex molecules: Combining molecular mechanics and continuum models. Acc Chem Res 33:889–897.

27. Qiu X, Kroeker A, He S, Kozak R, Audet J, Mbikay M, Chrétien M. 2016. Prophylactic efficacy of quercetin 3-β-O-D-glucoside against Ebola virus infection. Antimicrob Agents Chemother 60:5182–5188.

28. Diaz MO, Ziemin S, Le Beau MM, Pitha P, Smith SD, Chilcote RR, Rowley JD. 1988. Homozygous deletion of the α- and β1-interferon genes in human leukemia and derived cell lines. Proc Natl Acad Sci U S A 85:5259–5263.

29. Olejnik J, Nelson E V. 2017. Analyzing apoptosis induction and evasion in ebola virus-infected cellsMethods in Molecular Biology.

30. Gastaminza P, Whitten-Bauer C, Chisari F V. 2010. Unbiased probing of the entire hepatitis C virus life cycle identifies clinical compounds that target multiple aspects of the infection. Proc Natl Acad Sci 107:291–296.

31. Sheahan TP, Sims AC, Graham RL, Menachery VD, Gralinski LE, Case JB, Leist SR, Pyrc K, Feng JY, Trantcheva I, Bannister R, Park Y, Babusis D, Clarke MO, MacKman RL, Spahn JE, Palmiotti CA, Siegel D, Ray AS, Cihlar T, Jordan R, Denison MR, Baric RS. 2017. Broad-spectrum antiviral GS-5734 inhibits both epidemic and zoonotic coronaviruses. Sci Transl Med 9:eaal3653.

32. Abner E, Stoszko M, Zeng L, Chen H-C, Izquierdo-Bouldstridge A, Konuma T, Zorita E, Fanunza E, Zhang Q, Mahmoudi T, Zhou M-M, Filion GJ, Jordan A. 2018. A new quinoline BRD4 inhibitor targets a distinct latent HIV-1 reservoir for re-activation from other ‘shock’ drugs. J Virol JVI.02056-17.

33. Van De Klundert MAA, Zaaijer HL, Kootstra NA. 2016. Identification of FDA-approved drugs that target hepatitis B virus transcription. J Viral Hepat 23:191–201.

34. Esposito F, Tramontano E. 2014. Past and future. Current drugs targeting HIV-1 integrase and reverse transcriptase-associated ribonuclease H activity: Single and dual active site inhibitors. Antivir Chem Chemother 23:129–144.

35. Khiar S, Lucas-Hourani M, Nisole S, Smith N, Helynck O, Bourgine M, Ruffié C, Herbeuval JP, Munier-Lehmann H, Tangy F, Vidalain PO. 2017. Identification of a small molecule that primes the type i interferon response to cytosolic DNA. Sci Rep 7.

36. Jones M, Cunningham ME, Wing P, DeSilva S, Challa R, Sheri A, Padmanabhan S, Iyer RP, Korba BE, Afdhal N, Foster GR. 2017. SB 9200, a novel agonist of innate immunity, shows potent antiviral activity against resistant HCV variants. J Med Virol 89:1620–1628.

37. Zinzula L, Tramontano E. 2013. Strategies of highly pathogenic RNA viruses to

block dsRNA detection by RIG-I-like receptors: Hide, mask, hit. Antiviral Res 100:615–635.

38. Pizzolla A, Smith JM, Brooks AG, Reading PC. 2017. Pattern recognition receptor immunomodulation of innate immunity as a strategy to limit the impact of influenza virus. J Leukoc Biol 101:851–861.

39. Di Palma F, Daino GL, Ramaswamy VK, Corona A, Frau A, Fanunza E, Vargiu A V., Tramontano E, Ruggerone P. 2019. Relevance of Ebola virus VP35 homo-dimerization on the type I interferon cascade inhibition. Antivir Chem Chemother 27.

40. Jasenosky LD, Cadena C, Mire CE, Borisevich V, Haridas V, Ranjbar S, Nambu A, Bavari S, Soloveva V, Sadukhan S, Cassell GH, Geisbert TW, Hur S, Goldfeld AE. 2019. The FDA-Approved Oral Drug Nitazoxanide Amplifies Host Antiviral Responses and Inhibits Ebola Virus. iScience 19:1279–1290.

41. Zhao Z, Martin C, Fan R, Bourne PE, Xie L. 2016. Drug repurposing to target Ebola virus replication and virulence using structural systems pharmacology. BMC Bioinformatics 17:1–12.

42. Darapaneni V. 2014. Virion Protein 24 of Ebola Virus as a Potential Drug Target. Am J Curr Microbiol 3:14–22.

43. Setlur AS, Naik SY, Skariyachan S. 2017. Herbal Lead as Ideal Bioactive Compounds Against Probable Drug Targets of Ebola Virus in Comparison with Known Chemical Analogue : A Computational Drug Discovery Perspective. Interdiscip Sci Comput Life Sci 9:254–277.

44. Pinto AK, Williams GD, Szretter KJ, White JP, Proença-Módena JL, Liu G, Olejnik J, Brien JD, Ebihara H, Mühlberger E, Amarasinghe G, Diamond MS, Boon ACM. 2015. Human and Murine IFIT1 Proteins Do Not Restrict Infection of Negative-Sense RNA Viruses of the Orthomyxoviridae, Bunyaviridae, and Filoviridae Families. J Virol 89:9465–9476.

45. Umesh C V, Jamsheer AM, Prasad MA. 2018. The Role of Flavonoids in Drug Discovery- Review on potential applications. Res J Life Sci Bioinformatics, Pharm Chem Sci 4:70–77.

46. Johari J, Kianmehr A, Mustafa MR, Abubakar S, Zandi K. 2012. Antiviral activity of baicalein and quercetin against the Japanese encephalitis virus. Int J Mol Sci 13:16020–16045.

47. Zandi K, Teoh BT, Sam SS, Wong PF, Mustafa M, Abubakar S. 2011. Antiviral activity of four types of bioflavonoid against dengue virus type-2. Virol J 8:560.

48. Liu AL, Wang H Di, Lee SM, Wang YT, Du GH. 2008. Structure-activity relationship of flavonoids as influenza virus neuraminidase inhibitors and their in vitro anti-viral activities. Bioorganic Med Chem 16:7141–7147.

49. Bang S, Li W, Ha TKQ, Lee C, Oh WK, Shim SH. 2017. Anti-influenza effect of the major flavonoids from Salvia plebeia R.Br. via inhibition of influenza H1N1 virus neuraminidase. Nat Prod Res 32:1224–1228.

50. Esposito F, Sanna C, Del Vecchio C, Cannas V, Venditti A, Corona A, Bianco A, Serrilli AM, Guarcini L, Parolin C, Ballero M, Tramontano E. 2013. Hypericum hircinum L. Components as new single-molecule inhibitors of both HIV-1 reverse transcriptase-associated DNA polymerase and ribonuclease H activities. Pathog Dis 68:116–124.

51. Sanna C, Rigano D, Corona A, Piano D, Formisano C, Farci D, Franzini G, Ballero M, Chianese G, Tramontano E, Taglialatela-Scafati O, Esposito F. 2018. Dual HIV-1 reverse transcriptase and integrase inhibitors from Limonium morisianum Arrigoni, an endemic species of Sardinia (Italy). Nat Prod Res 33:1768–1803.

52. Zakaryan H, Arabyan E, Oo A, Zandi K. 2017. Flavonoids: promising natural compounds against viral infections. Arch Virol 162:12539–2551.

53. D'Andrea G. 2015. Quercetin: A flavonol with multifaceted therapeutic applications?

673 Fitoterapia 106:256–71.

674 54. Khachatoorian R, Arumugaswami V, Raychaudhuri S, Yeh GK, Maloney EM, Wang
675 J, Dasgupta A, French SW. 2012. Divergent antiviral effects of bioflavonoids on the
676 hepatitis C virus life cycle. Virology 433:346–355.

677 55. Dos Santos AE, Kuster RM, Yamamoto KA, Salles TS, Campos R, De Meneses
678 MDF, Soares MR, Ferreira D. 2014. Quercetin and quercetin 3-O-glycosides from
679 Bauhinia longifolia (Bong.) Steud. show anti-Mayaro virus activity. Parasites and
680 Vectors 7:130.

681 56. Kim Y, Narayanan S, Chang KO. 2010. Inhibition of influenza virus replication by
682 plant-derived isoquercetin. Antiviral Res 88:227–235.

683 57. Lani R, Hassandarvish P, Chiam CW, Moghaddam E, Jang J, Chu H, Rausalu K,
684 Merits A, Higgs S, Vanlandingham D, Bakar SA, Zandi K, Chu JJH, Rausalu K,
685 Merits A, Higgs S, Vanlandingham D, Abu Bakar S, Zandi K. 2015. Antiviral activity
686 of silymarin against chikungunya virus. Sci Rep 5:11421.

687 58. Lee M, Son M, Ryu E, Kang H, Shin YS, Kim JG, Kang BW, Cho H. 2015.
688 Quercetin-induced apoptosis prevents EBV infection. Oncotarget 6:12603–12624.

689 59. Bachmetov L, Gal-Tanamy M, Shapira A, Vorobeychik M, Giterman-Galam T,
690 Sathiyamoorthy P, Golan-Goldhirsh A, Benhar I, Tur-Kaspa R, Zemel R. 2012.
691 Suppression of hepatitis C virus by the flavonoid quercetin is mediated by inhibition
692 of NS3 protease activity. J Viral Hepat 19:e81–e88.

693 60. Granato M, Gilardini Montani MS, Zompetta C, Santarelli R, Gonnella R, Romeo MA,
694 D'Orazi G, Faggioni A, Cirone M. 2019. Quercetin interrupts the positive feedback
695 loop between STAT3 and IL-6, promotes autophagy, and reduces ROS, preventing
696 EBV-driven B cell immortalization. Biomolecules 9:482.

697 61. Yeh SL, Lin YC, Lin YL, Li CC, Chuang CH. 2016. Comparing the metabolism of
698 quercetin in rats, mice and gerbils. Eur J Nutr 55:413–422.

62. Baize S, Pannetier D, Oestereich L, Rieger T, Koivogui L, Magassouba N, Soropogui B, Sow MS, Keïta S, De Clerck H, Tiffany A, Dominguez G, Loua M, Traoré A, Kolié M, Malano ER, Heleze E, Bocquin A, Mély S, Raoul H, Caro V, Cadar D, Gabriel M, Pahlmann M, Tappe D, Schmidt-Chanasit J, Impouma B, Diallo AK, Formenty P, Van Herp M, Günther S. 2014. Emergence of Zaire Ebola Virus Disease in Guinea. N Engl J Med 371:1418–1425.

63. Mohamadi F, Richards NGJ, Guida WC, Liskamp R, Lipton M, Caufield C, Chang G, Hendrickson T, Still WC. 1990. Macromodel—an integrated software system for modeling organic and bioorganic molecules using molecular mechanics. J Comput Chem 11:440–467.

64. Halgren TA. 1996. Merck molecular force field. I. Basis, form, scope, parameterization, and performance of MMFF94. J Comput Chem 17:490–519.

65. Berman, H. M.; Westbrook, J.; Feng, Z.; Gilliland, G.; Bhat, T. N.; Weissig, H.; Shindyalov, I. N.; Bourne PE. 2000. The protein data bank. Nucleic Acids Res 28:235–242.

66. Kaminski GA, Friesner RA, Tirado-Rives J, Jorgensen WL. 2001. Evaluation and reparametrization of the OPLS-AA force field for proteins via comparison with accurate quantum chemical calculations on peptides. J Phys Chem B 105:6474–6487.

Figure legends

Figure 1. Inhibition of VP24 by Gossypetin, Taxifolin and Tricetin. (A) Chemical structures of Gossypetin, Taxifolin and Tricetin. (**B**) HEK293T cells were transfected with pISRE-luc, Renilla luciferase-thymidine kinase DNA (RL-TK) and pcDNA3.1 or VP24 expression plasmid. 24 h after transfection, cells were stimulated with IFN-α, and

725 Gossypetin, Taxifolin, Tricetin were added. Then, luciferase activity was measured.
726 Results are shown as percentage of ISRE expression in VP24 transfected cells over
727 empty vector control. Firefly luciferase activity is normalized to the Renilla luciferase
728 internal control. Error bars indicate the mean ± SD of at least three independent
729 experiments. *P< 0.05, **P< 0.01, asterisks indicate a significant difference (two-tailed
730 unpaired Student's t-test, n=3).
731
732 **Figure 2. Effect of screened flavonoids on EBOV VP24 inhibition of IFN signaling.**
733 **(A)** Chemical structures of Quercetin and Wogonin. **(B)** HEK293T cells were transfected
734 with pISRE-luc, RL-TK and pcDNA3.1 or EBOV VP24 expression plasmid. After 24 h, cells
735 were treated with IFN-α and compounds. After 8 h of stimulation, luciferase activity was
736 measured. Results are shown as percentage of ISRE expression in VP24 transfected cells
737 over pcDNA3.1 control. **(C** and **D)** After 24 h of cotransfection with pISRE-luc, RL-TK and
738 pcDNA3.1, HEK293T were stimulated with IFN-α and compounds. Results are shown as
739 percentage of ISRE expression in compounds treated cells over not treated control. Firefly
740 luciferase activity is normalized to the Renilla luciferase internal control. Error bars indicate
741 the mean ± SD of at least three independent experiments. *P< 0.05, **P< 0.01 and
742 ***P< 0.005, asterisks indicate a significant difference (two-tailed unpaired Student's t-test,
743 n=3).
744
745 **Figure 3. Quercetin dose-dependently inhibits VP24 IFN inhibitory function.** (**A**)
746 HEK293T cells were cotransfected with pISRE-luc, RL-TK and VP24 plasmid. 24 h after
747 transfection, cells were stimulated with IFN-α and Quercetin was added to VP24
748 cotransfected cells. After 8 h, cells were lysed, and luciferase was measured. Results are
749 shown as percentage of VP24 inhibitory activity on ISRE expression using as positive
750 control of inhibition (100%) cells not treated with Quercetin. Firefly luciferase activity was

751 normalized to the Renilla luciferase internal control. (**B**) HEK293T were treated with
752 Quercetin and cytotoxicity was measured. Results are shown as percentage of cells
753 counts treated with Quercetin over not treated cells. (**C**) HEK293T cells transfected with
754 pcDNA3.1 or VP24 plasmid. After 24 h, cells were stimulated with IFN-α and treated or not
755 with Quercetin (30 μM). After 24 h, total RNA was extracted, and RT-qPCR was
756 performed. Results are shown as percentage of ISG15 mRNA expression in VP24
757 cotransfected cells (treated or not with Quercetin) over empty vector control. Error bars
758 indicate the mean ± SD of three independent experiments. **P< 0.01, two-tailed unpaired
759 Student's t-test, n=3.
760
761 **Figure 4. Effect of Quercetin on VP24 inhibition of P-STAT1 nuclear translocation**.
762 (**A**) Row 1-2: Immunofluorescence of HEK293T cotransfected with empty vector (EV) not
763 stimulated (row 1) or stimulated (row 2) with IFN-α for 30 min. Row 3-4:
764 Immunofluorescence of HEK293T cotransfected with FLAG-tagged VP24 plasmid
765 stimulated with IFN-α and not treated (row 3) or treated (row 4) with Quercetin (30 μM).
766 Asterisk indicated P-STAT1 in the nucleus of a VP24 cell treated with Quercetin. All cells
767 were stained for FLAG and P-STAT1. Scale bar, 10 μm. (**B**) Percentage of nuclear P-
768 STAT1 within transfected cells expressing VP24. Error bars represent the mean of three
769 independent experiments. ****P< 0.0001, two-tailed unpaired Student's t-test, n=3.
770
771 **Figure 5.** (**A**) Three-dimensional representation of the putative binding mode obtained by
772 blind docking experiments of Quercetin into VP24. (**B**) Relative 2D representation of the
773 complexes stabilizing interactions. (**C**) Alignment of Quercetin-VP24 complex obtained by
774 docking experiment with VP24 – KPNα5 reported in 4U2X PDB model (9). (**D**) Schematic
775 representation of KPNA-VP24 co-IP experiment in presence of Quercetin (**E**) HEK293T

776 cells were cotransfected with an V5-tagged form of EBOV VP24 and FLAG-tagged KPNα1.
777 Empty vector was used as a negative control. At 24 h post-transfection, cells were lysed
778 and co-IP was performed using anti-FLAG magnetic beads (IP:FLAG). Immunoprecipitated
779 proteins were detected by Western blotting with antibodies to V5 (WB: V5) and FLAG
780 (WB:FLAG). The presence of transfected proteins in whole cell extracts (WCE) was
781 verified by detection with the corresponding antibodies. Bands quantification was
782 performed.
783
784 **Figure 6. Quercetin inhibits EBOV replication in HEK293T cells.** HEK293T (**A**) and
785 Vero E6 (**C**) cells were treated with DMSO, Quercetin (30 μM), Q3G (10 μM) or IFNα
786 (1000 IU/ml), and infected or not (NI) with EBOV Makona (MOI=0,1) and cultured for 72h.
787 Then, cells were harvested and analyzed by RT-qPCR for EBOV NP expression in cell
788 lysates. Supernatants from HEK293T (**B**) and Vero E6 cells (**D**) cultures were harvested
789 and analyzed by RT-qPCR for EBOV NP expression in supernatants. Results are
790 presented as a mean ± SE and statistical significances between DMSO-treated EBOV-
791 infected cells and Quercetin-, Q3G- and IFNα-treated EBOV-infected cells was analyzed
792 using One-Way ANOVA followed by Tukey's multiple comparisons test (* $P < 0.05$; ** $P <$
793 0.01; *** $P < 0.001$; **** $P < 0.0001$). Cell lysates from HEK293T (**E**) and Vero E6 (**F**) were
794 analyzed by Western blot analysis for caspase-3 and cleaved caspase-3 expression in cell
795 lysates.
796
797 **Figure 7.** (**A**) HEK293T VP24 transfected cells were stimulated with IFN-α and treated
798 with Quercetin and Q3G. After 8 h, luciferase was read. Results are shown as percentage
799 of VP24 inhibitory activity on ISRE expression using as positive control of inhibition (100%)
800 not treated cells. Error bars indicate the mean ± SD of three independent experiments; (**B**)

801 HEK293T transfected with pISRE-luc, RL-TK and pcDNA3.1, were treated with IFN-α and
802 Q3G. Results are shown as percentage of ISRE expression in Q3G treated cells over not
803 treated control. (**C**) HEK293T were treated with Q3G and cytotoxicity was measured.
804 Results are shown as percentage of cell viability in Q3G treated over not treated cells
805 (100%); (**D**) Immunofluorescence of HEK293T cotransfected with VP24 and treated with
806 IFN-α and Q3G. Asterisks indicate P-STAT1 in the nucleus of a VP24 cell treated with
807 Q3G. Signal of P-STAT1 was detected and percentage of positive cells for nuclear P-
808 STAT1 was calculated, **P< 0.01, two-tailed unpaired Student's t-test, n=3. Scale bar, 10
809 μm. (**E**) Three-dimensional representation of superimposed putative binding modes
810 obtained by blind docking experiments of Q3G (in orange) and Quercetin (in blue) into
811 VP24; (**F**) Alignment of Quercetin-VP24 and Q3G-VP24 complexes obtained by docking
812 experiments with VP24 and KPNα5 reported in 4U2X PDB model (9); (**G**) Co-IP of V5-
813 VP24 with KPNα1 in presence or not of Q3G. Bands quantification was performed.

A

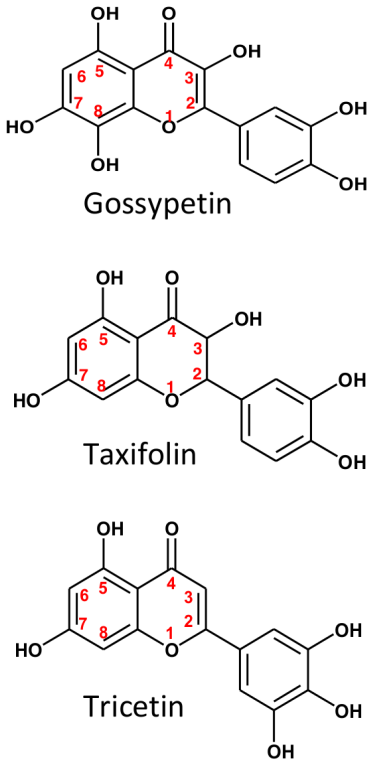

B